1 **A programmable probiotic encapsulation system enhances therapeutic delivery *in vivo***
2

3 Tetsuhiro Harimoto[1]*, Jaeseung Hahn[1]*, Yu-Yu Chen[1], Jongwon Im[1], Joanna Zhang[1], Nicholas
4 Hou[1], Fangda Li[2], Courtney Coker[1], Kelsey Gray[1], Nicole Harr[1], Sreyan Chowdhury[1,2], Kelly Pu[1],
5 Clare Nimura[1], Nicholas Arpaia[2,3], Kam Leong[1,4]†, Tal Danino[1,3,5]†
6

7 [1]Department of Biomedical Engineering, Columbia University, New York, NY 10027, USA.
8 [2]Department of Microbiology and Immunology, Vagelos College of Physicians and Surgeons,
9 Columbia University, New York, NY 10032, USA.
10 [3]Herbert Irving Comprehensive Cancer Center, Columbia University, New York, NY 10032, USA.
11 [4]Department of Systems Biology, Columbia University Medical Center, New York, NY 10032, USA.
12 [5]Data Science Institute, Columbia University, New York, NY 10027, USA.
13

14 *These authors contributed equally to this work.
15 †Co-corresponding authors. Email: kam.leong@columbia.edu, tal.danino@columbia.edu
16

17 **Abstract**
18 Recent advances in therapeutic modulation of human microbiota have driven new efforts to
19 engineer living microbial medicines using synthetic biology. However, a long-standing challenge
20 for live bacterial therapies is balancing the high dose required to achieve robust efficacy with the
21 potential for sepsis. Here, we developed a genetically encoded microbial encapsulation system
22 with tunable and dynamic expression of surface capsular polysaccharides to enhance therapeutic
23 delivery. Following a synthetic small RNA knockdown screen of the capsular biosynthesis
24 pathway, we constructed synthetic gene circuits that regulate bacterial encapsulation based on
25 sensing the levels of environmental inducer, bacterial density, and blood pH. The induced
26 encapsulation system enabled tunable immunogenicity and survivability of the probiotic
27 *Escherichia coli*, resulting in increased maximum tolerated dose and enhanced efficacy in murine
28 cancer models. Furthermore, triggering *in situ* encapsulation was found to increase microbial
29 translocation between mouse tumors, leading to efficacy in distal tumors. The programmable
30 encapsulation system demonstrates a new approach to control microbial therapeutic profiles *in
31 vivo* using synthetic biology.
32

33 **Main Text**
34 The microbiome plays numerous functional roles in human health and subsequently has led to
35 focused interest in the use of live bacteria to treat disease[1,2]. Since microbes can be engineered
36 as intelligent living medicines that sense and respond to environments, they can colonize niches
37 in the gastrointestinal tract[3,4], mouth[5], skin[6], lung[7], and tumors[8,9], and locally deliver therapeutics.
38 However, host toxicity from live bacteria has been shown to limit tolerated dose and efficacy, in
39 some cases leading to termination of clinical trials[10-13]. Moreover, unlike conventional drug carriers,
40 the unique abilities of bacteria to continuously proliferate, chemotax, and produce therapeutic
41 payloads in disease sites necessitates robust and temporal control of bacterial pharmacokinetics
42 *in vivo*. One approach to circumvent toxicity is the generation of genetic knockouts of
43 immunogenic bacterial surface antigens such as lipopolysaccharide (LPS), but this strategy can
44 result in permanent strain attenuation and reduced colonization, as seen in clinical trials of
45 bacteria cancer therapy[11,14,15]. Surface modulation has been widely utilized in cloaking drug
46 delivery vehicles[16], and thus an alternative strategy is the synthetic coating of microbial surfaces
47 with molecules such as alginate[17,18], chitosan[17], polydopamine[19], lipids[20-22], and nanoparticles[23].
48 However, these one-time, static modifications of bacteria do not allow for *in situ* modulation and
49 can lead to uncontrolled growth, off-target toxicity, or compromised cellular function resulting in
50 reduced efficacy.
51

52   Here, we present a tunable microbial surface engineering strategy using synthetic gene circuits
53   to dynamically control bacterial interactions with their surrounding environment. We focused on
54   bacterial surface capsular polysaccharides (CAP), a natural extracellular biopolymer that coats
55   the extracellular membrane and protects microbes from a variety of environmental conditions[24].
56   By applying a synthetic biology approach to engineer CAP biosynthesis, we constructed
57   programmable CAP expression systems that sense environmental cues and controllably
58   modulate the bacterial surface, thereby modulating bacterial interaction with antimicrobials,
59   bacteriophage, acidity, and host immunity. This design allows precise control over bacterial
60   immunogenicity and survivability *in vivo*, enabling novel drug delivery strategies such as
61   enhanced dosing and *in situ* trafficking to maximize therapeutic efficacy and safety (Fig. 1).

sRNA knockdown screen identifies key regulators of CAP synthesis

64   Since various bacteria have been utilized for therapeutic applications, we compared
65   immunogenicity and viability of several *E. coli* and *S. typhimurium* strains. Here *E. coli* Nissle 1917
66   (EcN), a probiotic strain with favorable clinical profiles[25], demonstrated high viability in human
67   whole blood with minimal cytokine induction (Supplementary Fig. 1a,b). Because the K5-type CAP
68   of EcN has been shown to alter interaction with host immune systems[26-29], we chose to genetically
69   modify its biosynthetic pathway[30,31]. K5-type CAP produced from EcN, also known as heparosan,
70   is composed of a polymer chain of alternating β-D-glucuronic acid (GlcA) and N-acetyl-α-D-
71   glucosamine (GlcNAc), attached to 3-deoxy-D-manno-oct-2-ulosonic acid (Kdo) linker (Fig. 2a).
72   Glycotransferases of *kfiABCD* genes polymerize alternating GlcA and GlcNAc subunits. *kpsCSFU*
73   genes are responsible for synthesis of the poly-Kdo linker on the terminal lipid, and CAP is
74   transported to the cellular surface by *kpsEDMT* genes. While individual functions of the CAP
75   genes have been investigated, engineering tunable and dynamic control of this system remains
76   unexplored.

78   We sought to identify key CAP genes capable of altering response to antibacterial factors
79   encountered during therapeutic delivery. To do so, we generated a library of knockdown (KD)
80   strains using synthetic small RNAs (sRNAs) that reduce expression of *kfi* and *kps* genes via
81   complementary binding to mRNAs[32]. To initially assess the impact of downregulating each gene,
82   we screened the growth of KD strains in (1) nutrient-rich media, (2) human whole blood, and (3)
83   CAP-targeting phage. Growth in nutrient-rich media showed little variation in maximum specific
84   growth rates (μ_m) from the wild-type EcN strain (expressing CAP) (Fig. 2b, Supplementary Fig.
85   2a), suggesting that the downregulation of the targeted genes in the CAP biosynthetic pathway
86   does not greatly affect the fitness of EcN in the absence of environmental threats. However, we
87   observed significantly reduced viability of KD strains compared to EcN after incubation in whole
88   blood for 0.5 hours (Supplementary Fig. 2b). After a 6-hour incubation in whole blood, KD strains
89   in CAP synthesis (*kfi* genes and *kpsFU*) exhibited lower viability compared to KD strains in CAP
90   transport (*kpsEDMT*) (Fig. 2b). To assess whether each gene KD causes a complete or partial
91   loss of CAP in KD strains, we used lytic bacteriophage ΦK1-5 that specifically binds to heparosan
92   of EcN[29,33]. Bacteria that express residual levels of heparosan CAP are susceptible to this phage,
93   but complete loss of CAP confers immunity. We quantified phage sensitivity of each strain by
94   measuring area under the curve of the phage-inoculated growth curve[34] and observed that sRNA
95   KD of most CAP genes did not alter phage sensitivity compared to control EcN (Fig. 2b,
96   Supplementary Fig. 2c), suggesting some level of CAP is still present in KD strains. To abrogate
97   the effect of residual CAP gene expression, we next constructed a library of knockout (KO) strains
98   by deleting CAP synthesis genes from EcN genome using Lambda Red recombineering system.
99   All *kfi* KO strains resulted in complete phage immunity (Supplementary Fig. 2d), supporting loss
100 of CAP expression. Importantly, KO strains demonstrated significantly increased blood sensitivity
101 (Supplementary Fig. 2e), indicating that CAP levels can be genetically tuned to alter sensitivities
102 to antibacterial factors.

103
104 On the basis of the above results, we chose to further characterize *kfiC*, a well-studied gene that
105 encodes an essential glycotransferase of GlcA[26,29]. Downregulation of *kfiC* via sRNA KD
106 sensitized bacteria in blood, suggesting its key role in regulating bacterial protection. Deletion of
107 *kfiC* resulted in the highest enhancement in blood sensitivity, indicating that the level of protection
108 can be altered by controlling gene expression. To confirm loss of CAP from the bacterial surface,
109 we characterized surface properties of EcN Δ*kfiC* strain. Phage plaque formation assay confirmed
110 complete immunity against ΦK1-5 (Fig. 2c). We also purified and detected bacterial
111 polysaccharides using sodium dodecyl sulfate–polyacrylamide gel electrophoresis (SDS-PAGE)
112 followed by CAP staining with alcian blue. Compared to EcN that produced strong staining with
113 alcian blue at ~180 kDa, EcN Δ*kfiC* produced no visible band (Supplementary Fig. 3a). We next
114 characterized the morphological changes in bacterial surface using transmission electron
115 microscopy (TEM) with ruthenium red staining. CAP was visible as an ~80 nm thick layer of
116 polysaccharides coating outside of the cellular membrane. In contrast, EcN Δ*kfiC* had diminished
117 size of the polysaccharides layer at ~40 nm (Fig. 2d, Supplementary Fig. 3a,b). We then
118 investigated capability of CAP to protect cells from wide range of antimicrobial factors. In addition
119 to the modified sensitivity to human whole blood and bacteriophage, EcN Δ*kfiC* demonstrated a
120 significant reduction in cellular protection against panels of antibiotics (spectinomycin, ampicillin,
121 gentamicin, kanamycin, streptomycin) and extreme acids (pH 2.5) compared to EcN
122 (Supplementary Fig. 4a-i). Finally, we evaluated general applicability of the approach in other
123 CAP systems. We deleted homologous genes in different *E. coli* strains expressing K1 and K5
124 CAP (*neuC* and *kfiC,* respectively) and showed alteration in environmental sensitivity
125 (Supplementary Fig. 5a-c). Together, these results demonstrate that loss of CAP modifies cellular
126 surface structure and protection against antimicrobial factors.
127
128 ***Construction of tunable and reversible programmable CAP***
129 We next constructed a programmable CAP system that can sense and respond to induction
130 stimuli and modulate cell surface properties. We cloned *kfiC* under the control of the *tac* promoter,
131 which can be activated with the small-molecule inducer isopropyl-b-D-thiogalactopyranoside
132 (IPTG) (Fig. 3a). Since the EcN genome encodes for constitutive *lacI* expression, we built a small
133 library of plasmids with various copy numbers of *kfiC* to optimize for tight regulation of CAP
134 production. EcN Δ*kfiC* transformed with the low (sc101 origin) copy number plasmid exhibited
135 complete immunity against ΦK1-5 (Supplementary Fig. 6a), indicating tight repression at the basal
136 level. Induction with IPTG rescued the phage sensitivity (Supplementary Fig. 6b), confirming
137 inducible modulation of CAP on cellular surface.
138
139 We examined tunability of this inducible CAP (iCAP) system by characterizing multiple induction
140 conditions. SDS-PAGE showed increase in CAP production from EcN carrying the iCAP system
141 (EcN iCAP) when incubated with elevating levels of IPTG (Fig. 3b). Co-incubation with ΦK1-5
142 also showed decreasing viability of EcN iCAP with elevating levels of IPTG (Supplementary Fig.
143 6c). We next used TEM to investigate the effect of the iCAP system on cell surface morphology
144 (Fig. 3d). Increasing levels of IPTG shifted the mean bacterial membrane thickness from 44 nm
145 to 81 nm, confirming tunable capability of the system. Intermediate iCAP activation at 100 nM
146 revealed a bimodal distribution of the membrane thickness, suggesting that *kfiC* regulates the
147 production level but not the length of the polysaccharide polymers. This result agreed with SDS-
148 PAGE data that showed no difference in migration of CAP band depending on IPTG concentration
149 (Fig. 3b).
150
151 We subsequently evaluated the dynamics of production and recovery of the iCAP system using
152 a similar approach. Upon addition of IPTG, elevated CAP production was observed over time on
153 SDS-PAGE, reaching near-maximum levels by 4 hours (Fig. 3c). Similarly, removal of IPTG

154 resulted in gradual decrease in CAP until complete repression by 6 hours. We also tested iCAP
155 dynamics via co-incubation with ΦK1-5. While uninduced EcN iCAP grew, induction with IPTG at
156 the start of co-incubation resulted in a rapid lysis event at 3.5 hours (Supplementary Fig. 6d),
157 demonstrating delayed CAP production with similar kinetics observed in SDS-PAGE. Collectively,
158 these data highlight the programmable capability of CAP modulation on the bacterial surface.
159
160 ### *Programmable protection from host immunity*
161 To build towards utilization of the programmable CAP system for therapeutic applications *in vivo*,
162 we first tested the ability to exogenously control bacterial viability in human whole blood containing
163 functional host bactericidal factors *in vitro*. Upon IPTG induction, we observed increased EcN
164 iCAP survival compared to non-induced control (Fig. 4a). Increasing IPTG levels improved
165 bacterial survival over a range of at least ~10^5 fold, highlighting the tunable capability of the
166 system. Since iCAP deactivation was observed after removing the inducer, we tracked bacterial
167 survival over time after transiently activating EcN iCAP at varying IPTG concentration. We were
168 able to modulate the rate of bacterial clearance from blood by titrating levels of IPTG (Fig. 4b).
169 Wildtype EcN persisted for >6 hours, while EcN Δ*kfiC* quickly decreased to the levels under the
170 limit of detection (LOD ~10^2 CFU/mL) within the first 0.5 hour. A protective role of CAP in mouse
171 whole blood was also observed (Supplementary Fig. 7a,b).
172
173 Autonomous systems that repress CAP expression upon sensing of specific conditions would be
174 highly useful to clear bacteria and ensure safety. As a proof of principle, we constructed genetic
175 circuits capable of sensing (1) bacterial overgrowth at colonized sites, and (2) acidosis associated
176 with sepsis[35] to prevent systemic bacterial growth and inflammation. For both CAP systems, we
177 placed *kfiC* under the control of *tac* promoter on the high (ColE1 origin) copy number plasmid to
178 express CAP despite endogenous *lacI* expression. To design a CAP system responsive to
179 bacterial overgrowth, we incorporated a quorum-sensing module where bacteria express *luxI*
180 gene to produce diffusible small molecule N-Acyl homoserine lactone (AHL). Upon reaching
181 critical population density, the AHL-sensing *pluxI* promoter drives expression of *lacI*, repressing
182 CAP production (Fig. 4c). We cultured the bacteria to stationary phase in LB media to simulate
183 bacterial overgrowth, and observed that this quorum-sensing CAP (qCAP) system resulted in
184 bacterial immunity against ΦK1-5. Control strains harboring a mutated *luxI* gene[36] were sensitive
185 to the phage, and exogenous addition of AHL molecule rescued bacterial immunity
186 (Supplementary Fig. 8a), confirming CAP repression via quorum-sensing circuit. To test the safety
187 feature of the system, we inoculated the bacteria in human whole blood. Rapid elimination of the
188 qCAP strain was observed after 2 hours while the control strain persisted (Fig. 4c), indicating
189 bacterial overgrowth sensitizes bacteria to immune clearance via qCAP. To sense acidosis, we
190 utilized a previously characterized pH-sensitive promoter pCadC. Membrane tethered
191 endogenous CadC protein is cleaved to activate pCadC promoter in an acidic environment which
192 drives expression of *lacI* to repress CAP production (Fig. 4d). While the bacteria carrying this
193 acidosis-sensing CAP (aCAP) system were sensitive to ΦK1-5 in a physiologically neutral
194 condition (pH 7.4), they were able to grow in the presence of ΦK1-5 in a pH level similar to severe
195 acidosis[37,38] (pH 6.8) (Supplementary Fig. 8b), indicating CAP repression upon sensing acidity.
196 When the aCAP strain was inoculated in human whole blood, we observed decreased levels of
197 bacteria in acidic condition (Fig. 4d, Supplementary Fig. 8c). These genetic circuits highlight
198 exogenous and autonomous control over bacterial CAP expression, allowing for programmable
199 bacteria sensitivity to host immune detection to enhance safety.
200
201 To investigate the effect of the programmable CAP system on bacterial interaction with individual
202 immune factors within whole blood, we assessed how CAP alterations modulated macrophage-
203 mediated phagocytosis and complement-mediated killing. To study phagocytosis, we incubated
204 EcN with murine bone marrow-derived macrophages. iCAP activation prior to co-incubation with

205 macrophages resulted in reduction in uptake of bacteria within macrophages compared to basal
206 control (Supplementary Fig. 9a,b), demonstrating controllable protection from cellular immune
207 recognition. Bacterial colony counting of macrophage lysates and fluorescence microscopy
208 imaging confirmed ~10-fold less phagocytosis with bacteria induced with IPTG compared to
209 uninduced control (Fig. 4e). To assess inflammatory response by the phagocytes, we co-cultured
210 EcN with THP-1 human monocytic cells and measured levels of TNFα, a major cytokine produced
211 in response to microbial detection. Presence of CAP reduced levels of TNFα (Fig. 4f), indicating
212 the ability of CAP to mask microbial recognition from the immune system. To study protection
213 against circulating host antimicrobials such as the complement system, we exposed EcN to
214 human plasma. Presence of CAP improved bacterial survival by at least ~10^5 fold (Supplementary
215 Fig. 10), demonstrating that CAP protects bacteria from soluble host bactericidal factors. Together,
216 these findings suggest the potential utility of the programmable CAP system to modulates a
217 multitude of host-microbe interactions *in vivo*.
218
219 ### *Transient CAP improves safety and efficacy of engineered probiotic therapy*
220 Intravenous (i.v.) delivery of bacteria allows access to various disease sites in the body; however,
221 systemic delivery of bacteria remains challenging because (1) rapid clearance by the host immune
222 system requires increased dosing, while (2) failure in bacteria clearance can lead to bacteremia
223 and sepsis. Since the programmable CAP system allowed temporal control over bacterial
224 protection and immunogenicity, we sought to improve bacterial delivery by initially protecting
225 bacteria during the delivery stage via CAP production, and subsequently allowing CAP decay to
226 clear them and ensure safety. To study the protective role of CAP *in vivo*, we first characterized
227 probiotic bioavailability and host health in mouse models (Fig. 5a). Upon i.v. administration of EcN
228 Δ*kfiC*, viable bacteria in blood circulation quickly dropped below the LOD (200 CFU/mL). In
229 contrast, EcN remained detectable during the first 4 hours (Supplementary Fig. 11a),
230 demonstrating the protective function of CAP *in vivo*. To examine the host response to
231 encapsulated (*i.e.*, wild type) *vs.* unencapsulated (*i.e.*, Δ*kfiC*) EcN, we measured levels of serum
232 TNFα and total white blood cell count. We detected lower levels of serum TNFα in the first hour
233 of EcN injection compared to EcN Δ*kfiC* injection (Fig. 5b), similar to the decreased TNFα
234 response observed in our *in vitro* assay. This short-term inflammatory response was resolved
235 within 24 hours for both bacterial strains. In contrast to the rapid resolution of TNFα response, we
236 detected elevated total white blood cell count after 24 hours of injection at higher level with EcN
237 compared to EcN Δ*kfiC* (Supplementary Fig. 11b). Neutrophil expansion accounted for the
238 majority of the immune response to encapsulated EcN (Fig. 5b), suggesting that the persistence
239 of CAP-expressing EcN poses a risk of prolonged bacteremia, which may result in systemic
240 inflammation and toxicity. Thus, while CAP can improve bioavailability, static protection may lead
241 to prolonged bacterial circulation in blood and pose toxicity risks.
242
243 We hypothesized that transient activation of the programmable CAP system can improve bacterial
244 delivery profiles by modulating maximum injectable dose, host toxicity, and biodistribution.
245 Inducing CAP expression prior to injection would improve bioavailability and mask cytokine
246 induction, and loss of CAP in the absence of the inducer *in vivo* would effectively clear bacteria
247 and minimize long-term immune responses. To test this strategy, we first i.v. administered
248 escalating doses of EcN iCAP and assessed host health and determined maximum tolerable
249 dose[39,40] (MTD) (Fig. 5c). At lower doses, EcN iCAP caused a smaller decrease in body weight
250 compared to EcN and EcN Δ*kfiC* with static cellular surface (*i.e.*, with or without CAP, respectively)
251 (Supplementary Fig. 12a,b). Importantly, EcN iCAP dramatically reduced toxicity compared to
252 EcN and EcN Δ*kfiC* at higher doses: EcN and EcN Δ*kfiC* caused severe end-point toxicity (death
253 or >15% loss of weight) to mice treated with doses above $1{\times}10^7$ CFU within 2 days, while no mice
254 showed severe toxicity following injection of pre-induced EcN iCAP at the same doses (Fig. 5d).
255 Based on these data, we computed a dose-toxicity curve and demonstrated that transiently

256 induced EcN iCAP results in ~10-fold higher MTD compared to EcN and EcN Δ*kfiC* (Fig. 5e). To
257 further study safety, we simulated a severe toxicity scenario by inducing sepsis by intraperitoneal
258 injection of bacteria[41]. At both high and low doses (10^7 and 10^6 CFU, respectively), we consistently
259 observed improved safety for EcN iCAP compared to EcN and EcN Δ*kfiC* (Supplementary Fig.
260 13a,b). Finally, to study bacteria biodistribution, we administered all groups of EcN at a matched
261 dose of 5×10^6 CFU via i.v. injection. Approximately 10-fold less EcN and EcN iCAP were found in
262 peripheral organs (liver and spleen) compared to EcN Δ*kfiC* (Supplementary Fig. 14), indicating
263 that initial induction of EcN iCAP was sufficient to provide protection from the mononuclear
264 phagocyte system. These data support that transient activation of iCAP improves probiotic
265 delivery and safety.
266
267 Since systemic bacterial delivery has been extensively used for cancer therapy, we next tested
268 whether the programmable CAP system can improve antitumor efficacy by permitting higher
269 doses (Fig. 5f). To engineer bacteria to deliver antitumor payloads, we cloned a gene encoding
270 pore-forming toxin, theta toxin (TT), previously shown to be effective as a bacterial cancer
271 therapy[42], in a high copy number plasmid (ColE1) with a stabilization mechanism for *in vivo*
272 applications (Axe/Txe system[43]). In a syngeneic CT26 colorectal cancer model, we intravenously
273 administered engineered EcN at the corresponding MTD of each strain (EcN, EcN Δ*kfiC*, and EcN
274 iCAP at 5×10^6, 1×10^7, and 5×10^7 CFU, respectively), along with a low dose of EcN iCAP at 5×10^6
275 CFU to match the MTD of EcN. Over the following days, bacterial accumulation in tumors was
276 observed by luminescence. Here, EcN iCAP MTD showed significantly higher signals in tumors
277 compared to all other groups (Fig. 5g). After bacterial administration, we observed that mice
278 treated with EcN MTD, EcN Δ*kfiC* MTD, and low dose EcN iCAP exhibited modest tumor growth
279 suppression compared to untreated group over 14 days. By contrast, single administration of EcN
280 iCAP MTD resulted in significant tumor growth suppression by ~400% compared to the untreated
281 group (Fig. 5h). While increased MTD enabled by transient activation of the iCAP system
282 improved therapeutic efficacy, body weight of animals between MTD groups remained similar
283 (Supplementary Fig. 15). We next compared efficacy of TT-producing EcN and EcN iCAP at MTD
284 in a genetically engineered spontaneous breast cancer model (MMTV-PyMT). EcN iCAP MTD
285 resulted in improved tumor growth suppression by ~100% compared to EcN MTD over 14 days
286 (Fig. 5i). Consistently, we observed higher bacterial signal in tumor from EcN iCAP compared to
287 EcN while body weight remains similar between the two treatment groups (Supplementary Fig.
288 16). To further explore the role of CAP on bacterial delivery to tumors *in vivo*, we built a
289 mathematical bacterial pharmacokinetics model. Our simulations suggested transient protection
290 of bacteria using the iCAP system could improve tumor specificity by minimizing persistence in
291 peripheral organs (*i.e.*, blood and liver), supporting our experimental observations
292 (Supplementary Fig. 17a). As a result, this approach allows for elevated bacterial doses, which
293 leads to increased tumor accumulation upon injection. Taken together, the iCAP system enables
294 increased tolerable bacterial doses and improved therapeutic efficacy.
295
296 ### *In situ CAP activation translocates EcN to distal tumors*
297 Intratumoral (i.t.) bacteria injection has been used as a route of delivery in clinical settings due to
298 higher therapeutic efficacy, dose titration capability, and improved safety profiles compared to
299 systemic injection[44-48]. One unique capability of i.t. delivery is the translocation of bacteria from
300 injected tumors to distal tumors[48], potentiating a novel route of safe bacterial delivery to
301 inaccessible tumors. However, continuous translocation coupled with long-term survival of
302 bacteria can pose a significant safety concern; thus transient *in situ* activation could allow for more
303 optimal utilization of this phenomena. To model this hypothesis, we simulated i.t. delivery and
304 showed that *in situ* induction of EcN iCAP within the tumor increases bacterial bioavailability in
305 circulation and facilitates bacterial translocation to distal tumors (Fig. 6a, Supplementary Fig. 17b).
306 We then tested this strategy via i.t. injection of uninduced EcN iCAP (*i.e.*, without CAP) into a

307 single tumor of mice harboring dual hind-flank CT26 tumors (Fig. 6b). To activate the iCAP system
308 *in situ*, mice were fed with water containing IPTG. After 3 days, we observed a marked increase
309 in bacterial translocation to distal tumors compared to uninduced bacteria (Fig. 6c, Supplementary
310 Fig. 18a,b). Biodistribution data showed tumor-specific translocation (Fig. 6d, Supplementary Fig.
311 18c), and mice exhibited minimal reductions in body weight (Supplementary Fig. 18d). Tracing
312 colonization kinetics using bioluminescent EcN confirmed the appearance of bacteria in distal
313 tumor 1 day following IPTG administration (Supplementary Fig. 19a). We next explored whether
314 this bacterial trafficking approach can be generalized in multiple clinically-relevant animal models.
315 We tested orthotopic breast cancer (mammary fat-pad 4T1) and MMTV-PyMT mouse models.
316 Consistently, we observed increased bacterial translocation to distal tumors via *in situ* activation
317 of iCAP in both tumor models (Fig. 6c, Supplementary Fig. 1b,c, Supplementary Fig. 20a-c,
318 Supplementary Fig. 21a-c). Notably, i.t. injection of EcN iCAP into a single tumor in the MMTV-
319 PyMT model resulted in microbial translocation to multiple distal tumors throughout the body
320 following IPTG induction. These results demonstrate the robustness of iCAP-mediated
321 translocation across a range of locations and tumor types.

322

323 We next delivered therapeutics to tumors using engineered EcN expressing the antitumor TT
324 payload. TT was cloned under the *luxI* promoter that is responsive to an inducer molecule AHL
325 orthogonal to IPTG (Fig. 6e). Following i.t. injection of therapeutic EcN into a single tumor in the
326 CT26 dual flank mouse model, translocation to uninjected tumors was controlled by feeding mice
327 with or without IPTG water. Another group of mice were given i.t. injection of EcN iCAP without
328 TT as non-therapeutic control. iCAP-mediated bacterial translocation was confirmed by bacterial
329 bioluminescence (Supplementary Fig. 22a-c). Subsequently, AHL was administered
330 subcutaneously to induce TT expression, and tumor growth was monitored. While PBS treatment
331 allowed tumor growth of ~400%, a reduction in the growth of tumors were observed when they
332 were directly injected with therapeutic EcN regardless of bacterial translocation. By contrast,
333 therapeutic efficacy in distal (uninjected) tumors was only observed when the mice were fed with
334 IPTG water followed by TT induction via subcutaneous injection of AHL (Fig. 6f, Supplementary
335 Fig. 23), demonstrating successful therapeutic delivery to distal tumors using the iCAP-mediated
336 bacterial translocation approach. Body weight quickly recovered to baseline within a few days
337 post administration for all conditions (Supplementary Fig. 24). Together, we provide a
338 demonstration of controllably translocating therapeutic bacteria and utilizing this strategy to treat
339 distal tumors *in vivo*.

340

341 ### *Conclusion*
342 We have demonstrated a synthetic biology approach for dynamic and tunable modulation of the
343 bacterial surface in the context of *in vivo* therapeutic delivery. Several biosensing circuits were
344 designed to allow for exogenous and autonomous regulation of CAP expression, which were
345 shown to enhance both safety and efficacy in multiple therapeutically-relevant scenarios. Taking
346 advantage of the natural evolution of the CAP system to interface with a multitude of environments,
347 we showed engineered bacterial interactions with host immunity, bacteriophage, antimicrobials
348 and acidity. Though we have explored the modulation of CAP density via *kfiC* in this study,
349 additional genes identified through our sRNA screen may also be used to achieve varied
350 sensitivities or to independently alter bacterial sensitivity to various environmental factors. For
351 example, *kfiB* and *kfiC* genes have been reported to differentially modulate bacterial interactions
352 with epithelial cells[29]. We have also shown that this approach can be applied to other strains of *E.*
353 *coli*. Since there exists over 80 distinct *E. coli* CAP systems[24,31] and many more in other species,
354 we envision CAP engineering to possess vast opportunities to controllably modulate microbial
355 surface properties for therapeutic delivery.

356

357 Despite recent preclinical progress with bacterial therapies, dose-limiting toxicity has been a long-
358 standing challenge, slowing efforts for clinical translation. Early works by William Coley in the 19th
359 century had observed tumor regression upon injections of a live bacterial cocktail[49], but this
360 approach was largely unsafe due to potential risks of infections and inflammatory side effects.
361 More recently, several clinical trials using genetically attenuated bacterial strains observed dose-
362 limiting toxicities. For example, systemic administration of attenuated *Salmonella typhimurium*
363 strain (VNP20009) at or higher than tolerable dose led to tumor colonization in < 20% of patients,
364 and resulted in no objective regression in a phase I clinical trial[11]. While the recent focus of
365 synthetic biology has been the engineering of various therapeutic payloads to increase efficacy,
366 strategies to improve bacterial delivery has been limited. We utilized on-demand CAP system to
367 controllably protect probiotic EcN from immune clearance, and demonstrated an ~10-fold
368 increase in the systemically injectable tolerated dose *in vivo*. As a result, transient expression of
369 CAP was able to safely enhance bacterial delivery and suppress rapidly growing syngeneic
370 colorectal tumors with a single i.v. administration. Given that humans are 250-fold more sensitive
371 to endotoxins compared to mice[50], we expect our results to have important implications in the
372 clinical translation of bacterial therapies. Since the CAP system is orthogonal to other bacterial
373 surface structures such as LPS, phospholipids, and flagellum[51], synergistic combinations of these
374 systems could further improve the programmability and immunogenicity of bacterial therapy, and
375 warrant future investigation.
376
377 We further devised the programmable CAP system to facilitate translocation of bacteria to distal
378 tumors, demonstrating a novel delivery strategy with advantageous safety profiles. Comparing
379 across different tumor types, we noted leakier translocation of bacteria in 4T1 and PyMT-MMTV
380 models, suggesting tumor type, location, or vascularization may play a role in bacterial escape
381 from the tumor microenvironment. Regardless, *in situ* activation of the programmable CAP system
382 opens the possibility of utilizing programmable translocation of therapeutic bacteria to
383 inaccessible disease sites including metastatic tumors. Transient *in situ* activation could allow for
384 colonization of newly formed tumors with reduced accessibility. As humarns are more sensitive
385 to bacteria compared to mice, we expect that the programmable CAP system will be far more
386 effective in human than mice at controlling bioavailability of bacteria in circulation. In addition, the
387 ability to transiently increase circulating bacteria from colonized tumor may allow safe sampling
388 of bacteria without the need for an invasive tumor biopsy while preventing excessive leakage of
389 bacteria that could cause bacteremia and systemic infection. More broadly, we envision that *in*
390 *situ* control over bacterial CAP may be utilized to provide further safeguards during bacterial
391 therapy such as sensitization of bacteria with antibiotics[52,53] and phage therapy[54].
392
393 In addition to clear applications within bacteria cancer therapy, the utility of the programmable
394 CAP system can be extended to other clinical settings. For example, we showed that CAP
395 provides protection from acids which could potentially protect orally-delivered probiotics during
396 transit through the gastric environment and facilitate intestinal colonization[55]. Beyond delivery,
397 altering surface immunogenicity may also be utilized therapeutically to modulate the host immune
398 landscape in the tumors and gut[56,57]. The platform described here could also be used as a model
399 system to study the role of CAP and other surface structures on pathogen colonization in the host
400 environment[58,59]. Aside from model systems and clinical applications, the programmable CAP
401 system may provide a general platform for a programmable interface with various environments.
402 As microbial deployment in various applications continue to advance, robust control over microbial
403 interaction with complex surroundings will ensure safe and effective implementation of engineered
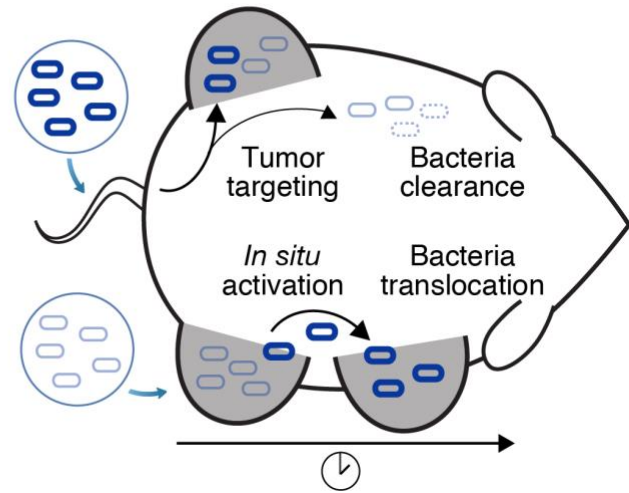404 microbes.
405
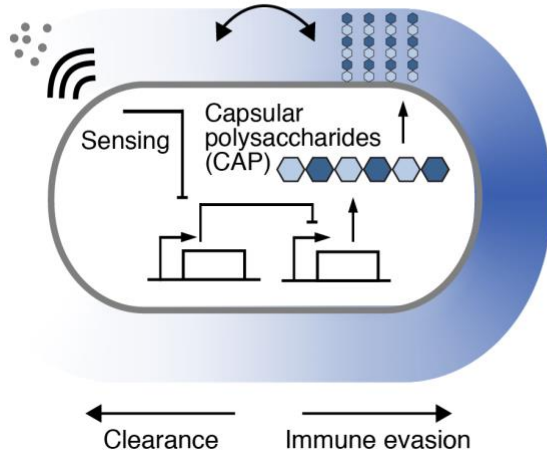
Figure 1: Programmable capsular polysaccharides (CAP) system for control over bacterial encapsulation and *in vivo* delivery profiles. We engineered the biosynthetic pathway of bacterial CAP for tunable and dynamic surface modulation of the probiotic *E. coli* Nissle 1917 with synthetic gene circuits. The CAP system modulates bacterial immunogenicity and survivability *in vivo*. By balancing these factors, the programmable CAP system is capable of reducing toxicity related to systemic bacterial administration and enables inducible bacterial translocation between tumors.
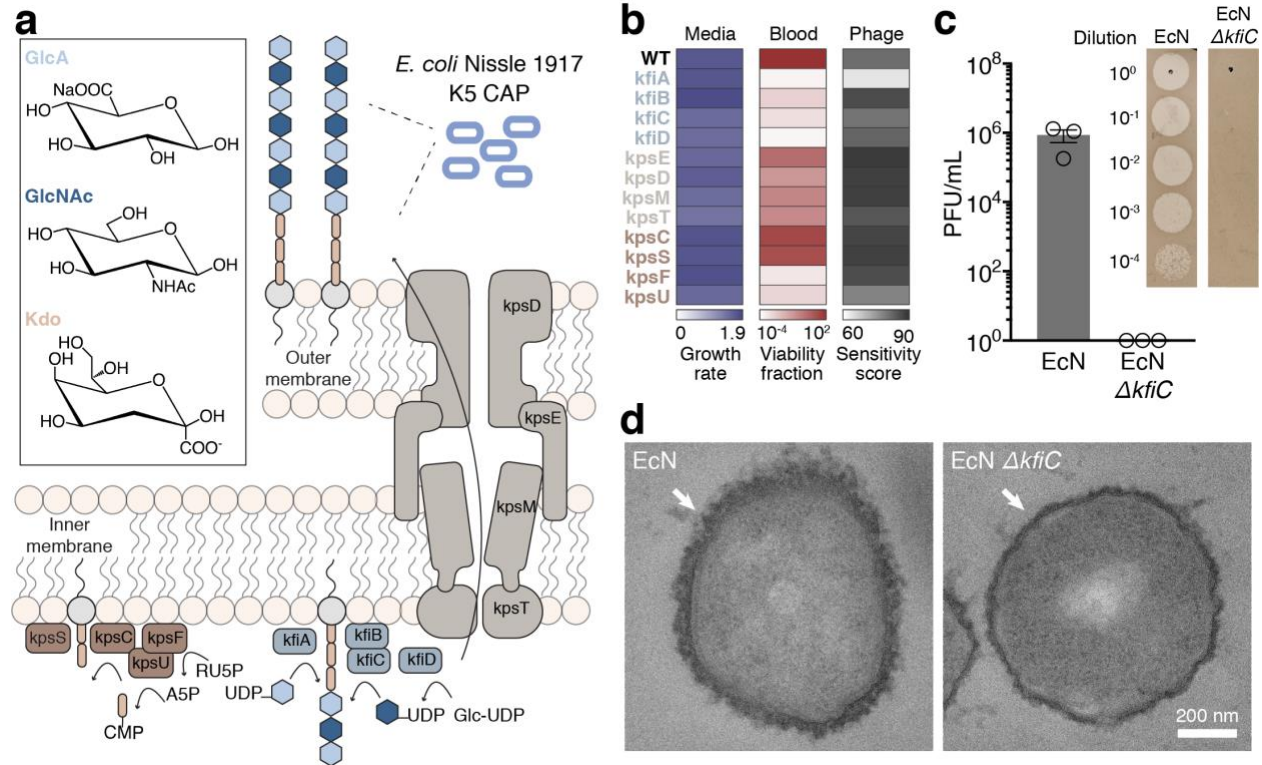
418
419
420 **Figure 2: sRNA knockdown screen identifies key genes in capsular polysaccharides**
421 **(CAP) biosynthesis. a,** Schematics of K5 CAP biosynthesis in EcN. CAP is composed of an
422 alternating polymer chain of GlcA and GlcNAc connected to a poly-KDO linker. Subsequently
423 CAP is transported from the inner bacteria membrane to the outer membrane. **b,** Quantification
424 of microbial growth parameters of EcN knockdown (KD) strains in nutrient, blood, or phage
425 containing media. Growth rate denotes maximum specific growth rate (hour^{-1}) obtained by fitting
426 growth curve to measured OD600 over time. Blood viability is defined as fraction of bacterial
427 CFU after 6 hours incubation in human blood over inoculated bacterial CFU. Phage sensitivity is
428 calculated by area under the curve of bacterial turbidity over 6 hours of incubation with LB
429 media containing ΦK1-5. **c,** Phage sensitivity of EcN and EcN Δ*kfiC*. Plaque forming assay
430 demonstrates complete absence of infection and lysis in EcN Δ*kfiC*. The representative images
431 show difference between serially-diluted plaque forming units (PFU) of bacteria with and without
432 CAP. **d,** TEM images showing CAP encapsulation of the cellular outer surface. *kfiC* knockout
433 results in the absence of CAP nanostructure on the cell surface of EcN Δ*kfiC*. White arrows
434 indicate cell surface.
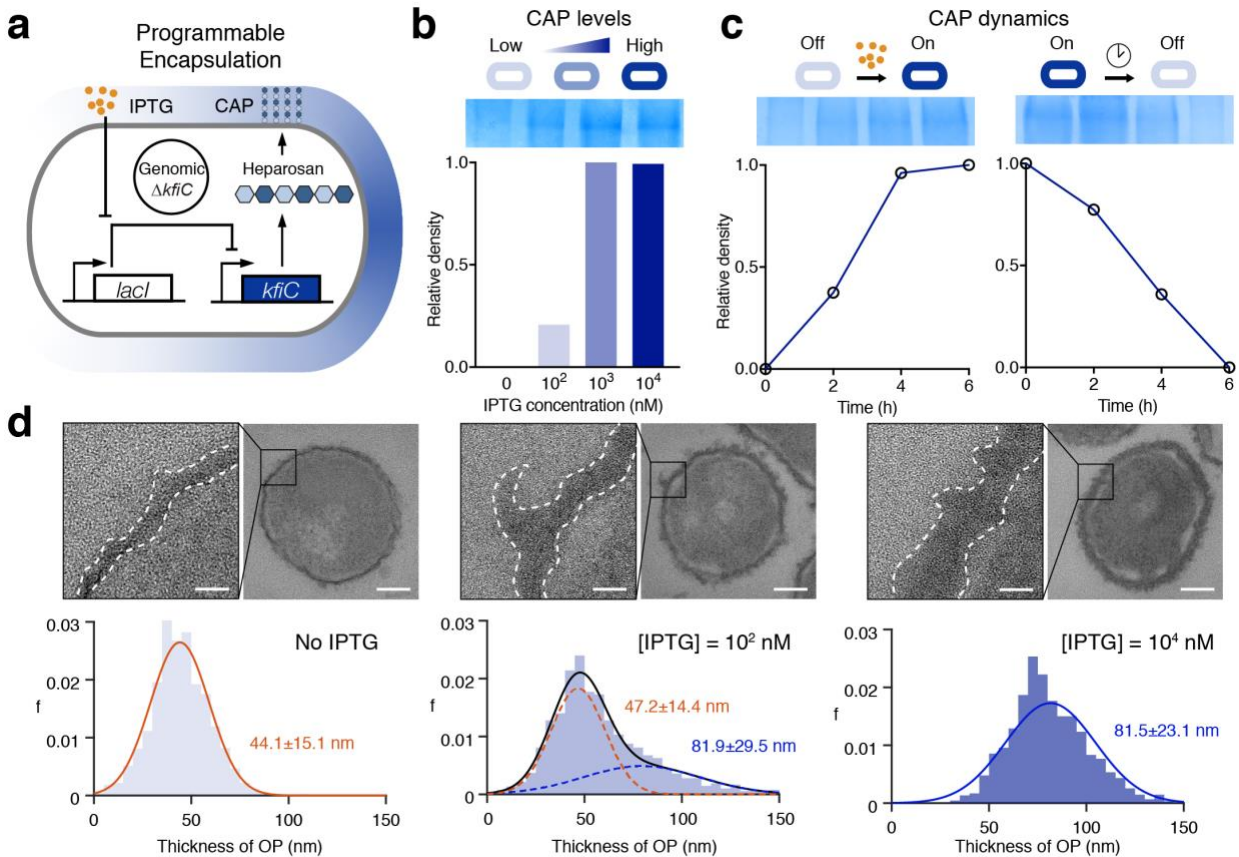
Figure 3: Design and characterization of the inducible capsular polysaccharides (iCAP) system. a, Inducible gene circuit diagram whereby the *kfiC* gene was cloned under the control of a *lac* promoter to allow inducible CAP expression via the small molecule IPTG. Copy number of the *kfiC* gene was modified to minimize basal *kfiC* expression. **b,** SDS-PAGE gel stained with Alcian blue showed elevating levels of CAP production corresponding to the IPTG concentration (top). The densitometric analysis of CAP bands demonstrated that CAP production reaches maximum at approximately 1 µM IPTG (bottom). **c,** SDS-page gels and densitometric analysis show CAP kinetics upon induction (left) and decay (right). **d,** Ruthenium red-stained TEM images showing change in CAP in titrating IPTG concentration. Histograms reveal shift in cellular outer layer thickness as IPTG concentration increases. Insets show representative images of bacteria and zoomed outer surface structure. Dotted lines indicate inner (white) and outer (gray) perimeters of CAP. Scale bar is 40 nm (left) or 200 nm (right) in each inset.
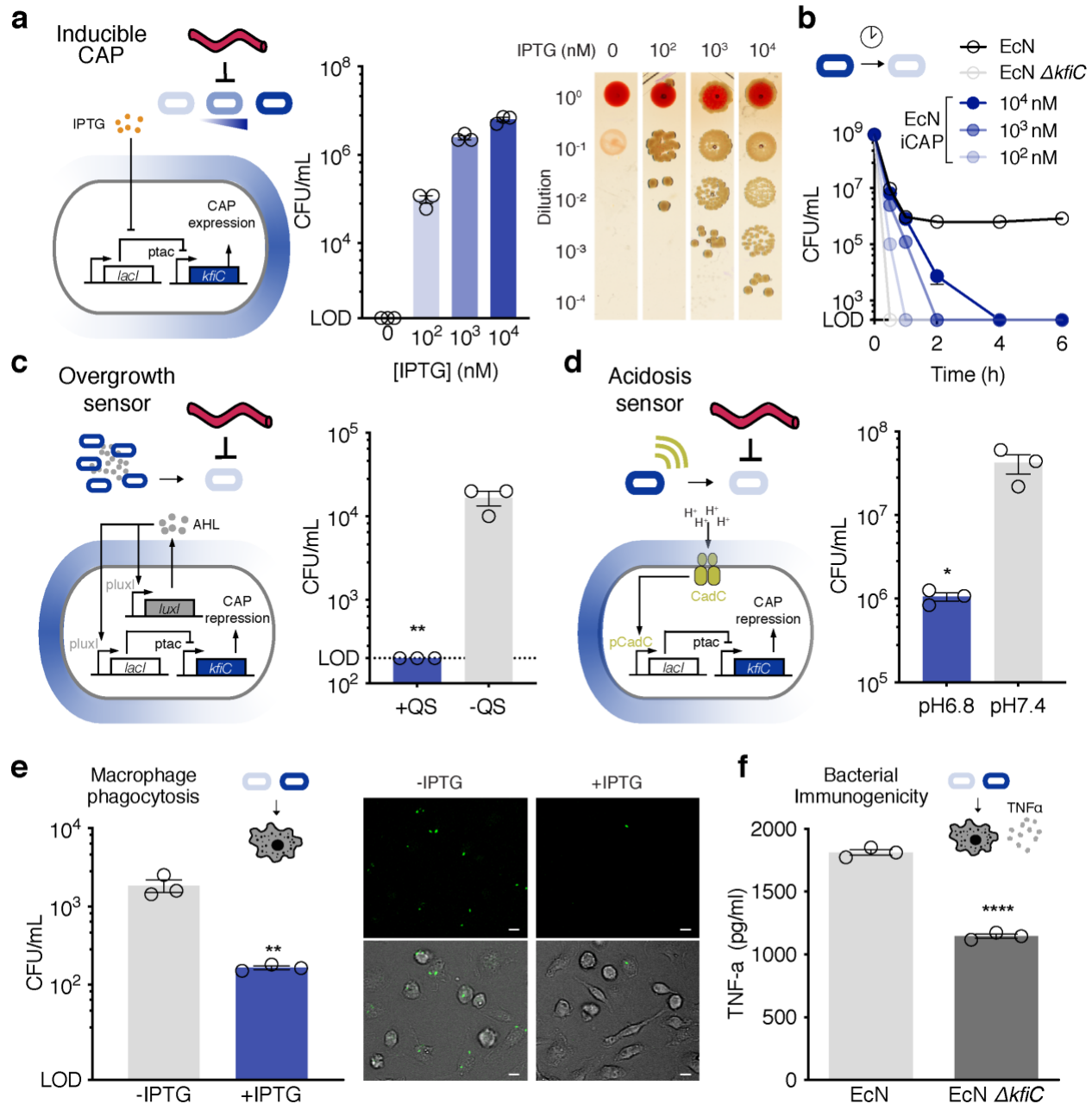
Figure 4: Tunable interaction of the programmable capsular polysaccharides (CAP) system with host immune factors. a, Elevating levels of CAP activation with IPTG enabled corresponding increase in bacterial survival in human whole blood (left). Representative images of bacteria spotted on LB-agar plate after 1 hour incubation in human whole blood (right). **b,** Survival kinetics using varying levels of IPTG induction prior to incubation with human whole blood. LOD at 2×10^2 CFU/mL. **c,** Gene circuit diagram for repression of CAP upon sensing bacterial overgrowth (left). Quorum sensing (QS) *luxI* gene produces diffusible AHL molecules which activates the pluxI promoters. *lacI* gene is placed under the control of pluxI promoter, repressing *kfiC* expression upon reaching quorum. Reduced bacterial survival was achieved after 2 hours inoculation in human whole blood (right; **P = 0.007, unpaired t-test). -QS denotes a control strain with mutated *luxI* gene. LOD at 2×10^2 CFU/mL. **d,** Gene circuit diagram for repression of CAP upon sensing blood acidosis (left). *lacI* gene is placed under the control of pCadC acid-sensitive

468 promoter, repressing *kfiC* expression upon sensing acidity. Reduced bacterial survival was
469 achieved 4 hours post inoculation in human whole blood at physiologically relevant neutral
470 (pH7.4) and acidic (pH6.8) conditions (right; *P = 0.02, unpaired t-test). **e,** BMDMs were co-
471 cultured with activated or non-activated bacteria for 30 minutes and lysed to enumerate
472 phagocytosed bacterial number. The representative fluorescence microscopy images show
473 decrease in bacteria (GFP, top) in phagocytes (Brightfield, bottom) upon CAP activation (**P =
474 0.007, unpaired t-test). Scale bar is 10 µm. **f,** CAP contribution to immune recognition. ELISA of
475 TNFα showed a decrease in cytokine production by THP-1 cells incubated with EcN compared to
476 the cells incubated with EcN Δ*kfiC* (****P < 0.0001, unpaired t-test). All error bars represent
477 standard error of mean (SEM) over three independent samples. Limit of detection (LOD) at 2×10^2
478 CFU/mL in all panels.
479
480
481
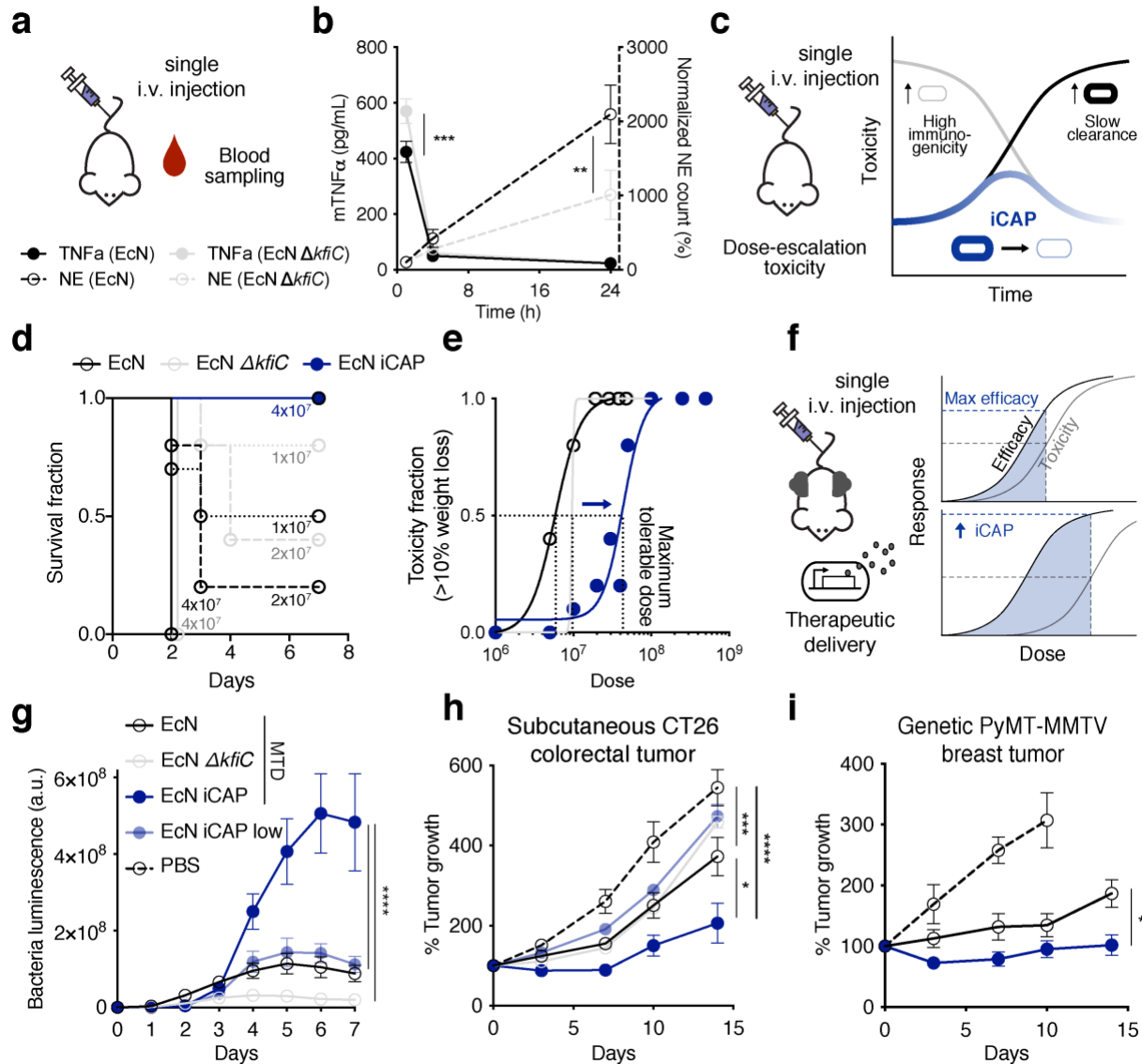
Figure 5: Transient capsular polysaccharides (CAP) activation improves systemic bacterial delivery and efficacy *in vivo*. a, Evaluation of host response after bacterial administration. 5×10⁶ bacteria were systemically delivered to BALB/c mice by i.v. injection, and cheek blood was collected at 1, 4, and 24 hours post injection (p.i.). **b,** Change in TNFα levels (solid line) and neutrophil count (dotted line) after bacterial injection. EcN induced lower levels of initial TNFα spikes compared to EcN Δ*kfiC* (***P = 0.0007, two-way ANOVA with Sidak's multiple comparisons test; n = 5 per group). EcN induced greater levels of neutrophil expansion compared to EcN Δ*kfiC*. Difference in neutrophil levels were observed after 24 hours p.i. (**P = 0.005, two-way ANOVA with Sidak's multiple comparisons test; n = 5 per group). **c,** Safety evaluation upon i.v. bacteria injection with elevating dosage. BALB/c mice were i.v. administered with EcN iCAP, EcN, or EcN Δ*kfiC* at dosage ranging from 5x10⁶ to 5x10⁸ CFU. EcN iCAP was pre-induced with 10 µM IPTG and allowed for gradual attenuation of CAP over time to minimize toxicity. **d,** Survival curve after bacterial administration. All animals injected with 4x10⁷ CFU of EcN or EcN Δ*kfiC* succumbed within 2 days (>15% body weight reduction). All mice survived after injection with 4x10⁷ CFU of EcN iCAP (n ≥ 5 mice per group). **e,** Dose-toxicity curve. Transient activation of iCAP increased maximum tolerable dose (MTD = 4.4x10⁷ CFU) compared to EcN (5.8x10⁶ CFU)

500   or EcN Δ*kfiC* (9.6x10^6 CFU). MTD was calculated based on TD50 for exhibiting moderate toxicity
501   (>10% body weight drops p.i.; Nonlinear regression with least squares fit; n ≥ 5 per group). **f,**
502   Therapeutic bacteria administration at MTD to improve antitumor efficacy. Mice bearing tumors
503   were i.v. injected with EcN MTD, EcN Δ*kfiC* MTD, EcN iCAP MTD (pre-induced with 10 μM IPTG),
504   or EcN iCAP low (pre-induced with 10 μM IPTG) expressing antitumor theta-toxin at 5x10^6, 1x10^7,
505   5x10^7, or 5x10^6 CFU, respectively. **g,** Bacterial growth trajectories in subcutaneous CT26 tumors
506   after intravenous delivery *in vivo.* Each line represents average of bacterial growth trajectories in
507   tumors quantified by bacterial luminescence over time for each bacterial strain injected. Mice
508   injected with EcN iCAP MTD showed higher bacterial luminescence in tumors compared to mice
509   injected with EcN MTD, EcN Δ*kfiC* MTD, and EcN iCAP low (****$P < 0.0001$, Two-way ANOVA
510   with Turkey's multiple comparison test; n = 14, 13, 9, and 13 tumors, respectively, for EcN MTD,
511   EcN Δ*kfiC* MTD, EcN iCAP MTD and EcN iCAP low groups). Luminescence values are
512   normalized to basal luminescence of individual strains. **h,** Therapeutic efficacy measured by
513   relative tumor size over time in a syngeneic CT26 model. EcN iCAP MTD demonstrated highest
514   tumor growth suppression (****$P < 0.0001$, ***$P = 0.0008$, **$P = 0.003$; two-way ANOVA with
515   Tukey's multiple comparison test; n = 14, 13, 9, 13 and 11 tumors, respectively, for EcN MTD,
516   EcN Δ*kfiC* MTD, EcN iCAP MTD, EcN iCAP low, and PBS groups). **i,** Therapeutic efficacy
517   measured by relative tumor size over time in a genetically engineered spontaneous breast cancer
518   (MMTV-PyMT) mouse model. Tumor growth was measured by calipering three orthotopic regions
519   in mammary glands (upper left, upper right, and bottom). EcN iCAP MTD demonstrated higher
520   tumor growth suppression than EcN MTD (*$P = 0.0197$; two-way ANOVA; n = 15, 15, and 9 tumors,
521   respectively, for EcN MTD, EcN iCAP MTD, and PBS groups. Mice in PBS groups reached study
522   endpoint 10 days p.i.). All error bars represent SEM.
523
524
525
526
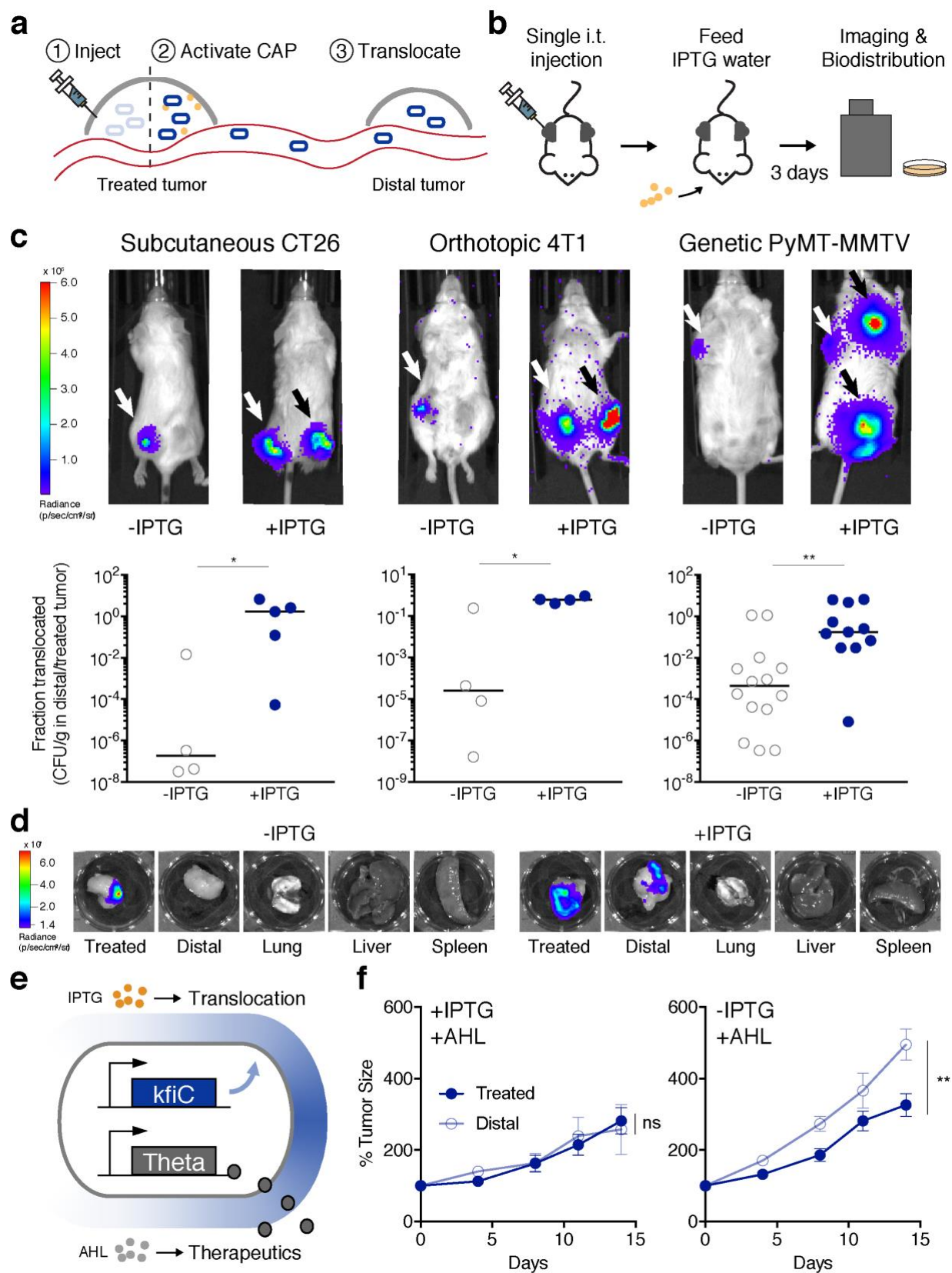
Figure 6: *In situ* **activation of the programmable capsular polysaccharides (CAP) enables bacterial translocation and drug delivery to distal tumors. a,** Schematics of iCAP-mediated

530   bacterial translocation. EcN are injected into one tumor (treated tumor). iCAP activation enables
531   bacteria translocation to distal tumors. **b,** Mice harboring multiple tumors are injected with EcN
532   iCAP into a single tumor (treated tumor). Subsequently, mice are fed 10 mM IPTG water to
533   activate iCAP *in situ*. Mice are imaged daily for bacterial bioluminescence to track tumor
534   colonization in tumors. To quantify bacterial biodistribution, organs are harvested and bacterial
535   colonies are counted after 3 days. **c,** Inducible translocation of EcN iCAP to distal tumors in CT26
536   syngeneic (left), 4T1 orthotopic (middle), and MMTV-PyMT genetically engineered (right) mouse
537   tumor models. Representative IVIS images showing bacterial translocation *in vivo*. White arrows
538   indicate location of bacterial injection. Black allows indicate location of bacterial translocation.
539   Translocation is quantified by fraction of bacteria found in distal tumor compared to treated tumor.
540   Bacteria number is measured by performing biodistribution for CFU/g enumeration. iCAP
541   activation showed marked increase in bacterial translocation (*P = 0.032, *P = 0.029, **P = 0.003,
542   Mann-Whitney test). **d,** Representative images of *ex vivo* organ images taken with IVIS showing
543   bacterial tumor translocation in 4T1 orthotopic mouse model. **e,** Schematics of engineered EcN
544   capable of programmable translocation and therapeutic expression. Therapeutic production is
545   externally controlled by an inducer AHL. The engineered EcN was injected into a single tumor
546   and IPTG-induced to translocate to distal tumors, and AHL-induced to deliver therapeutics. **f,**
547   Therapeutic efficacy in treated and distal CT26 tumors measured by relative tumor growth over
548   time. Bacteria were injected into a single treated tumor. The translocation was controlled by IPTG
549   water. 3 days p.i., AHL was administered to induce therapeutic expression. Distal tumor growth
550   was suppressed only when therapeutic bacteria were able to translocate (n.s. P = 0.83, **P =
551   0.004, two-way ANOVA with Bonferroni posttest, n = 6, 5 for both treated and distal tumors,
552   respectively). All error bars represent SEM.
553

Reference

1   Ruder, W. C., Lu, T. & Collins, J. J. Synthetic biology moving into the clinic. *Science* **333**, 1248-1252, doi:10.1126/science.1206843 (2011).

2   Lam, K. N., Alexander, M. & Turnbaugh, P. J. Precision Medicine Goes Microscopic: Engineering the Microbiome to Improve Drug Outcomes. *Cell Host Microbe* **26**, 22-34, doi:10.1016/j.chom.2019.06.011 (2019).

3   Riglar, D. T. *et al.* Engineered bacteria can function in the mammalian gut long-term as live diagnostics of inflammation. *Nat Biotechnol* **35**, 653-658, doi:10.1038/nbt.3879 (2017).

4   Mao, N., Cubillos-Ruiz, A., Cameron, D. E. & Collins, J. J. Probiotic strains detect and suppress cholera in mice. *Sci Transl Med* **10**, doi:10.1126/scitranslmed.aao2586 (2018).

5   Cagetti, M. G. *et al.* The use of probiotic strains in caries prevention: a systematic review. *Nutrients* **5**, 2530-2550, doi:10.3390/nu5072530 (2013).

6   Nakatsuji, T. *et al.* A commensal strain of Staphylococcus epidermidis protects against skin neoplasia. *Sci Adv* **4**, eaao4502, doi:10.1126/sciadv.aao4502 (2018).

7   Dickson, R. P., Erb-Downward, J. R. & Huffnagle, G. B. The role of the bacterial microbiome in lung disease. *Expert Rev Respir Med* **7**, 245-257, doi:10.1586/ers.13.24 (2013).

8   Forbes, N. S. Engineering the perfect (bacterial) cancer therapy. *Nature Reviews Cancer* **10**, 785-794 (2010).

9   Zhou, S., Gravekamp, C., Bermudes, D. & Liu, K. Tumour-targeting bacteria engineered to fight cancer. *Nat Rev Cancer* **18**, 727-743, doi:10.1038/s41568-018-0070-z (2018).

10   Flickinger, J. C., Jr., Rodeck, U. & Snook, A. E. Listeria monocytogenes as a Vector for Cancer Immunotherapy: Current Understanding and Progress. *Vaccines (Basel)* **6**, doi:10.3390/vaccines6030048 (2018).

11   Toso, J. F. *et al.* Phase I study of the intravenous administration of attenuated Salmonella typhimurium to patients with metastatic melanoma. *J Clin Oncol* **20**, 142-152, doi:10.1200/JCO.2002.20.1.142 (2002).

12   Sanders, M. E. *et al.* Safety assessment of probiotics for human use. *Gut Microbes* **1**, 164-185, doi:10.4161/gmic.1.3.12127 (2010).

13   Yelin, I. *et al.* Genomic and epidemiological evidence of bacterial transmission from probiotic capsule to blood in ICU patients. *Nat Med* **25**, 1728-1732, doi:10.1038/s41591-019-0626-9 (2019).

14   Low, K. B. *et al.* Lipid A mutant Salmonella with suppressed virulence and TNFalpha induction retain tumor-targeting in vivo. *Nat Biotechnol* **17**, 37-41, doi:10.1038/5205 (1999).

15   Wang, C. Z., Kazmierczak, R. A. & Eisenstark, A. Strains, Mechanism, and Perspective: Salmonella-Based Cancer Therapy. *Int J Microbiol* **2016**, 5678702, doi:10.1155/2016/5678702 (2016).

16   Mitchell, M. J. *et al.* Engineering precision nanoparticles for drug delivery. *Nat Rev Drug Discov* **20**, 101-124, doi:10.1038/s41573-020-0090-8 (2021).

17   Anselmo, A. C., McHugh, K. J., Webster, J., Langer, R. & Jaklenec, A. Layer-by-Layer Encapsulation of Probiotics for Delivery to the Microbiome. *Adv Mater* **28**, 9486-9490, doi:10.1002/adma.201603270 (2016).

18   Li, Z. H. *et al.* Biofilm-Inspired Encapsulation of Probiotics for the Treatment of Complex Infections. *Advanced Materials* **30**, doi:ARTN 1803925
10.1002/adma.201803925 (2018).

19   Chen, W. *et al.* Bacteria-Driven Hypoxia Targeting for Combined Biotherapy and Photothermal Therapy. *ACS Nano* **12**, 5995-6005, doi:10.1021/acsnano.8b02235 (2018).

20   Cao, Z., Wang, X., Pang, Y., Cheng, S. & Liu, J. Biointerfacial self-assembly generates lipid membrane coated bacteria for enhanced oral delivery and treatment. *Nat Commun* **10**, 5783, doi:10.1038/s41467-019-13727-9 (2019).

21   Cao, Z., Cheng, S., Wang, X., Pang, Y. & Liu, J. Camouflaging bacteria by wrapping with cell membranes. *Nat Commun* **10**, 3452, doi:10.1038/s41467-019-11390-8 (2019).

22   Qiao, Y. *et al.* Engineered algae: A novel oxygen-generating system for effective treatment of hypoxic cancer. *Sci Adv* **6**, eaba5996, doi:10.1126/sciadv.aba5996 (2020).

23   Hu, Q. L. *et al.* Engineering Nanoparticle-Coated Bacteria as Oral DNA Vaccines for Cancer Immunotherapy. *Nano Lett* **15**, 2732-2739, doi:10.1021/acs.nanolett.5b00570 (2015).

24   Cress, B. F. *et al.* Masquerading microbial pathogens: capsular polysaccharides mimic host-tissue molecules. *FEMS Microbiol Rev* **38**, 660-697, doi:10.1111/1574-6976.12056 (2014).

25   Sonnenborn, U. Escherichia coli strain Nissle 1917-from bench to bedside and back: history of a special Escherichia coli strain with probiotic properties. *FEMS Microbiol Lett* **363**, doi:10.1093/femsle/fnw212 (2016).

26   Burns, S. M. & Hull, S. I. Comparison of loss of serum resistance by defined lipopolysaccharide mutants and an acapsular mutant of uropathogenic Escherichia coli O75:K5. *Infect Immun* **66**, 4244-4253 (1998).

27   Hafez, M. *et al.* The K5 capsule of Escherichia coli strain Nissle 1917 is important in mediating interactions with intestinal epithelial cells and chemokine induction. *Infect Immun* **77**, 2995-3003, doi:10.1128/IAI.00040-09 (2009).

28   Hafez, M., Hayes, K., Goldrick, M., Grencis, R. K. & Roberts, I. S. The K5 capsule of Escherichia coli strain Nissle 1917 is important in stimulating expression of Toll-like receptor 5, CD14, MyD88, and TRIF together with the induction of interleukin-8 expression via the mitogen-activated protein kinase pathway in epithelial cells. *Infect Immun* **78**, 2153-2162, doi:10.1128/IAI.01406-09 (2010).

29   Nzakizwanayo, J. *et al.* Disruption of Escherichia coli Nissle 1917 K5 Capsule Biosynthesis, through Loss of Distinct kfi genes, Modulates Interaction with Intestinal Epithelial Cells and Impact on Cell Health. *Plos One* **10**, doi:ARTN e0120430
10.1371/journal.pone.0120430 (2015).

30   Wang, Z., Dordick, J. S. & Linhardt, R. J. Escherichia coli K5 heparosan fermentation and improvement by genetic engineering. *Bioeng Bugs* **2**, 63-67, doi:10.4161/bbug.2.1.14201 (2011).

31   Whitfield, C. & Roberts, I. S. Structure, assembly and regulation of expression of capsules in Escherichia coli. *Mol Microbiol* **31**, 1307-1319, doi:10.1046/j.1365-2958.1999.01276.x (1999).

659 32   Na, D. *et al.* Metabolic engineering of Escherichia coli using synthetic small
660   regulatory RNAs. *Nat Biotechnol* **31**, 170-174, doi:10.1038/nbt.2461 (2013).
661 33   Hafez, M. *et al.* The K5 Capsule of Escherichia coli Strain Nissle 1917 Is Important
662   in Mediating Interactions with Intestinal Epithelial Cells and Chemokine Induction.
663   *Infection and Immunity* **77**, 2995-3003, doi:10.1128/Iai.00040-09 (2009).
664 34   Xie, Y., Wahab, L. & Gill, J. J. Development and Validation of a Microtiter Plate-
665   Based Assay for Determination of Bacteriophage Host Range and Virulence.
666   *Viruses* **10**, doi:10.3390/v10040189 (2018).
667 35   Maciel, A. T., Noritomi, D. T. & Park, M. Metabolic acidosis in sepsis. *Endocr Metab*
668   *Immune Disord Drug Targets* **10**, 252-257, doi:10.2174/187153010791936900
669   (2010).
670 36   Hanzelka, B. L., Stevens, A. M., Parsek, M. R., Crone, T. J. & Greenberg, E. P.
671   Mutational analysis of the Vibrio fischeri LuxI polypeptide: critical regions of an
672   autoinducer synthase. *J Bacteriol* **179**, 4882-4887, doi:10.1128/jb.179.15.4882-
673   4887.1997 (1997).
674 37   Allyn, J. *et al.* Prognosis of patients presenting extreme acidosis (pH <7) on
675   admission to intensive care unit. *J Crit Care* **31**, 243-248,
676   doi:10.1016/j.jcrc.2015.09.025 (2016).
677 38   Acharya, A. P., Rafi, M., Woods, E. C., Gardner, A. B. & Murthy, N. Metabolic
678   engineering of lactate dehydrogenase rescues mice from acidosis. *Sci Rep* **4**, 5189,
679   doi:10.1038/srep05189 (2014).
680 39   Le Tourneau, C., Lee, J. J. & Siu, L. L. Dose escalation methods in phase I cancer
681   clinical trials. *J Natl Cancer Inst* **101**, 708-720, doi:10.1093/jnci/djp079 (2009).
682 40   Aston, W. J. *et al.* A systematic investigation of the maximum tolerated dose of
683   cytotoxic chemotherapy with and without supportive care in mice. *BMC Cancer* **17**,
684   684, doi:10.1186/s12885-017-3677-7 (2017).
685 41   Nemzek, J. A., Hugunin, K. M. & Opp, M. R. Modeling sepsis in the laboratory:
686   merging sound science with animal well-being. *Comp Med* **58**, 120-128 (2008).
687 42   Harimoto, T. *et al.* Rapid screening of engineered microbial therapies in a 3D
688   multicellular model. *Proc Natl Acad Sci U S A* **116**, 9002-9007,
689   doi:10.1073/pnas.1820824116 (2019).
690 43   Fedorec, A. J. H. *et al.* Two New Plasmid Post-segregational Killing Mechanisms
691   for the Implementation of Synthetic Gene Networks in Escherichia coli. *Iscience*
692   **14**, 323-+, doi:10.1016/j.isci.2019.03.019 (2019).
693 44   Roberts, N. J. *et al.* Intratumoral injection of Clostridium novyi-NT spores induces
694   antitumor responses. *Sci Transl Med* **6**, 249ra111,
695   doi:10.1126/scitranslmed.3008982 (2014).
696 45   Nemunaitis, J. *et al.* Pilot trial of genetically modified, attenuated Salmonella
697   expressing the E. coli cytosine deaminase gene in refractory cancer patients.
698   *Cancer Gene Ther* **10**, 737-744, doi:10.1038/sj.cgt.7700634 (2003).
699 46   Charbonneau, M. R., Isabella, V. M., Li, N. & Kurtz, C. B. Developing a new class
700   of engineered live bacterial therapeutics to treat human diseases. *Nat Commun*
701   **11**, 1738, doi:10.1038/s41467-020-15508-1 (2020).
702 47   Silverstein, M. J., DeKernion, J. & Morton, D. L. Malignant melanoma metastatic
703   to the bladder. Regression following intratumor injection of BCG vaccine. *JAMA*
704   **229**, 688 (1974).

705   48   Kocijancic, D. *et al.* Local application of bacteria improves safety of Salmonella -
706   mediated tumor therapy and retains advantages of systemic infection. *Oncotarget*
707   **8**, 49988-50001, doi:10.18632/oncotarget.18392 (2017).
708   49   Kienle, G. S. Fever in Cancer Treatment: Coley's Therapy and Epidemiologic
709   Observations. *Glob Adv Health Med* **1**, 92-100, doi:10.7453/gahmj.2012.1.1.016
710   (2012).
711   50   Copeland, S. *et al.* Acute inflammatory response to endotoxin in mice and humans.
712   *Clin Diagn Lab Immunol* **12**, 60-67, doi:10.1128/CDLI.12.1.60-67.2005 (2005).
713   51   Augustin, L. B. *et al.* Salmonella enterica Typhimurium engineered for nontoxic
714   systemic colonization of autochthonous tumors. *J Drug Target* **29**, 294-299,
715   doi:10.1080/1061186X.2020.1818759 (2021).
716   52   van Pijkeren, J. P. *et al.* A novel Listeria monocytogenes-based DNA delivery
717   system for cancer gene therapy. *Hum Gene Ther* **21**, 405-416,
718   doi:10.1089/hum.2009.022 (2010).
719   53   Zheng, D. W. *et al.* Optically-controlled bacterial metabolite for cancer therapy. *Nat*
720   *Commun* **9**, 1680, doi:10.1038/s41467-018-03233-9 (2018).
721   54   Lemire, S., Yehl, K. M. & Lu, T. K. Phage-Based Applications in Synthetic Biology.
722   *Annu Rev Virol* **5**, 453-476, doi:10.1146/annurev-virology-092917-043544 (2018).
723   55   Tahoun, A. *et al.* Capsular polysaccharide inhibits adhesion of Bifidobacterium
724   longum 105-A to enterocyte-like Caco-2 cells and phagocytosis by macrophages.
725   *Gut Pathog* **9**, 27, doi:10.1186/s13099-017-0177-x (2017).
726   56   Duong, M. T., Qin, Y., You, S. H. & Min, J. J. Bacteria-cancer interactions: bacteria-
727   based cancer therapy. *Exp Mol Med* **51**, 1-15, doi:10.1038/s12276-019-0297-0
728   (2019).
729   57   Lebeer, S., Vanderleyden, J. & De Keersmaecker, S. C. Host interactions of
730   probiotic bacterial surface molecules: comparison with commensals and
731   pathogens. *Nat Rev Microbiol* **8**, 171-184, doi:10.1038/nrmicro2297 (2010).
732   58   Sorg, R. A., Gallay, C., Van Maele, L., Sirard, J. C. & Veening, J. W. Synthetic
733   gene-regulatory networks in the opportunistic human pathogen Streptococcus
734   pneumoniae. *Proc Natl Acad Sci U S A* **117**, 27608-27619,
735   doi:10.1073/pnas.1920015117 (2020).
736   59   Siggins, M. K. *et al.* Extracellular bacterial lymphatic metastasis drives
737   Streptococcus pyogenes systemic infection. *Nat Commun* **11**, 4697,
738   doi:10.1038/s41467-020-18454-0 (2020).
739

1   **Materials and Methods**
2
3   ***Bacterial strains and culturing***
4   The host strain used in this study was *Escherichia coli* Nissle 1917 (EcN) that naturally expresses
5   K5 capsular polysaccharide (CAP) containing a genomically integrated erythromycin-resistance
6   *luxCDABE* cassette for bacterial bioluminescence tracking *in vivo*. For all strains used in this study,
7   please refer to Table S1. All bacteria were grown with appropriate antibiotics selection (100 μg/mL
8   ampicillin, 50 μg/mL kanamycin, 25 μg/mL chloramphenicol, 50 μg/mL erythromycin) in LB media
9   (Sigma-Aldrich) at 225 RPM or on LB-agar plates containing 1.5% agar at 37°C.
10
11   ***Construction of plasmids and gene circuits***
12   To construct a knockdown library, plasmids with sRNA targeting each gene of the CAP
13   biosynthetic pathway were prepared using Gibson Assembly. The sRNA sequences were
14   designed to be complementary and bind to the 24-neucleotide sequence of the target gene coding
15   sequence spanning the ribosome binding site and the start codon[1,2]. A plasmid template was
16   prepared by PCR-amplifying backbone (pTH05) using primers (pTH05_for and pTH05_rev), and
17   the single-stranded DNA for sRNA against genes in CAP biosynthesis were inserted (*kfiA, kfiB,*
18   *kfiD, kpsC, kpsS, kpsF, kpsU, kpsE, kpsD, kpsT, kpsM*), and transformed into Mach1 competent
19   cells (Invitrogen). CAP gene circuits and the therapeutic plasmids were constructed in a similar
20   manner. Genes of interest were obtained by synthesizing oligos or gBlock from IDT, or PCR-
21   amplification (*kfiC* gene was obtained via colony PCR from EcN). Subsequently, plasmids were
22   constructed using Gibson Assembly or using standard restriction digest and ligation cloning, and
23   transformed into Mach1 competent cells (Invitrogen).
24
25   ***Construction of knockout strains***
26   EcN was transformed to carry Lambda Red helper plasmid (pKD46)[3]. Transformants were grown
27   in 50 mL LB at 30°C with chloramphenicol to an OD600 of 0.4 and made electrocompetent by
28   washing three times with ice cold MilliQ water and concentrating 150-fold in 15% glycerol.
29   Chloramphenicol-resistance cassette was prepared by PCR with primers flanked by sequence
30   within each target gene followed by gel purification and resuspension in MilliQ water.
31   Electroporation was performed using 50 μL of competent cells and 10-100 ng of DNA. Shocked
32   cells were added to 1mL SOC, incubated at 30°C for 1 hour with 20 μL arabinose, and incubated
33   at 37°C for 1 hour. Cells were then plated on LB plates with chloramphenicol and incubated in
34   37°C overnight. Colonies were picked the next day to obtain knockout strains including Δ*kfiC*
35   strain (EcN Δ*kfiC*).
36
37   ***Characterization of CAP strains sensitivity to phages, antibiotics, and acids***
38   To perform plaque forming assay, bacteria were plated onto LB agar plates to make a lawn and
39   allowed to dry under fire. 10 μL of serial diluted ΦK1-5 phage (Molineux, University of Texas,
40   Austin) was spotted onto the plates and allowed to dry. Plates were incubated at 37°C overnight
41   and inspected the next day for plaque forming unit (PFU) counting. Similar phage plaque forming
42   assay were performed for K1 and K5 type *E. coli* strains.
43
44   To assess bacterial growth in liquid culture, overnight cultures of EcN, EcN Δ*kfiC*, or EcN iCAP
45   strains were calibrated into OD600 of 1.0, and 100 μL of each was transferred into 96-well plate
46   (Corning). 1 μL of 10^8 PFU ΦK1-5 phage, or antibiotics of indicated concentrations were added to
47   each well. The samples were incubated at 37°C with shaking in Tecan plate reader, and the
48   OD600 was measured every 20 min. For bacterial growth in low pH condition, LB media adjusted
49   to pH2.5 using HCl, bacteria were incubated at 37°C for 1 hour, followed by serial dilution and
50   plating on a LB agar plate for CFU enumeration.
51

Characterization of CAP using SDS-PAGE

CAP was purified via the chloroform-phenol extraction as previously described[4,5]. Briefly, 3 mL of overnight bacteria cultures were harvested the next day and further sub-cultured in 50 mL LB broth in the presence or absence of 0.1 M IPTG for indicated lengths of time. Bacteria concentrations were adjusted to the same level across samples via OD600 before centrifugation. Pellets were collected and resuspended in 150 µL of water. An equal amount of hot phenol (65°C) was added, and the mixtures were vortexed vigorously. The mixtures were then incubated at 65°C for 20 minutes, followed by chloroform extraction (400 µL) and centrifugation. The CAP were detected by alcian blue staining as previously reported[5–7]. Briefly, following SDS-PAGE electrophoresis (4-20% gradient), the gel was fixed in fixing solution (25% ethanol, 10% acetic acid in water) for 15 minutes while shaking at room temperature. The gel was then incubated in alcian blue solution (0.125% alcian blue in 25% ethanol, 10% acetic acid in water) at room temperature for 2 hours while shaking before de-stained overnight in fixing solution. CAP was visualized as alcian blue stained bands on the resulting gel.

Visualization of CAP using TEM

Bacteria were grown overnight in LB media with appropriate antibiotics before being processed for imaging. For EcN iCAP, a 1:100 dilution in LB with antibiotics was made the following day and grown in 37°C shaker until OD600 = 0.1–0.4 (mid-log phase), and varying concentrations of IPTG were added for further incubation for 6 hours before being processed. The cultures were spun down at 300 relative centrifugal force (rcf) for 10 min and embedded in 2% agarose. Each agarose gel fragment was cut into a cube with 2-mm edge and placed in a 1.5-mL centrifuge tube. The samples embedded in agarose were fixed and stained via protocols previously reported[8]. Briefly, the samples were fixed with 2% paraformaldehyde and 2.5% glutaraldehyde in osmotically adjusted buffer (0.1 M sodium cacodylate, 0.9 M sucrose, 10 mM $CaCl_2$, 10 mM $MgCl_2$) with 0.075% ruthenium red and 75 mM lysine acetate for 20 min on ice. The samples were washed with osmotically adjusted buffer containing 0.075% ruthenium red twice and further fixed with 1% osmium tetroxide in osmotically adjusted buffer containing 0.075% ruthenium red for an hour on ice. The samples were washed three times in water with 5 min incubation between each wash and dehydrated in increasing concentrations of ethanol (50%, 70%, and 100%) on ice for 15 min per step. The samples were washed one more time in 100% ethanol and embedded in increasing concentrations of Spurr's resin (33% and 66%) diluted in ethanol for 30 min per step and overnight in 100% Spurr's resin. The samples were moved to fresh Spurr's resin the next day and polymerized at 65°C overnight before sectioned using SORVALL MT-2B Ultramicrotome to ~70 nm. The sample sections were placed on TEM grids (Ted Pella; 01800F) and stained using UranyLess (EMS). The sample grids were imaged using FEI Talos 200 TEM.

TEM image processing and data analysis of polysaccharide layer

The image processing of TEM images was performed using ImageJ, and the data analysis was done using MATLAB. Due to low signal-to-noise ratio of the TEM images resulting from thinly sectioned bacteria samples stained using ruthenium red, Gaussian blur was used to reduce the noise and help determine boundary of polysaccharide layer. Polysaccharide layer was selected and transformed into binary image using threshold function. Some portion of boundary of polysaccharide layer was manually outlined when the thresholding function could not determine where the boundary is. The resulting binary image of polysaccharide layer was used to identify the centroid and measure distribution of polysaccharide thickness in respect to the centroid. For each sample, five representative images were used to measure the polysaccharide thickness and the measurements were aggregated to form histograms. The resulting histograms were fitted with Gaussian curves to extract mean and standard deviation of polysaccharide layer thickness.

In vitro whole blood bactericidal assays

103 EcN, EcN *ΔkfiC,* or EcN iCAP bacterial cultures were grown overnight in LB broth with appropriate
104 antibiotics and IPTG concentrations. The cultures were spun down at 3000 rcf for 5 min and
105 resuspended in 1 mL sterile PBS. They were further normalized to an OD600 of 1 with sterile
106 PBS. 150 µL of blood from the single donor human whole blood or murine (BALB/c) whole blood
107 (Innovative Research) were aliquoted into 3 wells/strain in a 96-well plate. 1.5 µL of bacteria were
108 added to each well and incubated at 37°C. At various time points, the plate was taken out, and a
109 serial dilution of each sample was prepared in PBS. The dilutions were plated on LB agar plates
110 with erythromycin. The agar plates were incubated at 37°C overnight and inspected the next day
111 for CFU counting.
112
113 ***Phagocytosis assays***
114 The phagocytosis assays were performed via protocols as previously reported[9,10]. Briefly, bone
115 marrow derived macrophages (BMDM) were thawed on a 15 cm non-TC treated petri dish and
116 cultured in RPMI with 10% FBS and MCSF for 4 days before experiment. On the 4th day, BMDMs
117 were collected, counted and diluted to 2×10^5 cells/mL in RPMI with 10% FBS (without antibiotics).
118 Afterwards, 1 mL of the new mixture was plated per well (2×10^5 cells) in a 24-well TC-treated
119 plate and cultured overnight. Media in the 24-well BMDM plate was removed the next day, and 1
120 mL of EcN iCAP constitutively expressing GFP with or without IPTG induction were resuspended
121 in RPMI with 10% FBS without antibiotics was added into each well at MOI of 100. The co-culture
122 was incubated for 30 min at 37°C followed by rigorous washing with PBS at least 3 times. 1 mL
123 of RPMI with 10% FBS and gentamicin (30 µg/mL) was added to each well, followed by live
124 imaging under confocal microscopy. 0.1 M IPTG was added to EcN iCAP with IPTG induction the
125 entire time. Then, the BMDMs were lysed with 0.5% TritonX in PBS and lysates were collected
126 and plated on LB agar with erythromycin followed by overnight incubation at 37°C. Colonies were
127 counted the next day. ImageJ was used to count the number of macrophages, engulfed bacterial
128 cells, and macrophages containing engulfed bacterial cells from the confocal images. The
129 phagocytic index was calculated according to the following formula: phagocytic index = (total
130 number of engulfed bacterial cells/total number of counted macrophages) × (number of
131 macrophages containing engulfed bacterial cells/total number of counted macrophages) × 100.
132
133 ***Determination of TNF-alpha response***
134 THP-1 cells (ATCC) were maintained in RPMI-1640 supplemented with 10% FBS, 2 mM L-
135 glutamine, 100 µg/mL streptomycin, 100 µg/mL penicillin, and 0.1% mercaptoethanol at 37°C and
136 5% CO_2. Cells were passaged every 72 hours. For cell quantification and viability analysis, cells
137 were stained using trypan blue stain. For *in vitro* TNF-alpha assay, THP-1 was resuspended at a
138 concentration of 1×10^6 cells/mL in RPMI-1640 supplemented with 10% FBS and 0.1%
139 gentamycin. 300 µL of cell suspension was transferred into each well of a 24-well plate. 3 µL of
140 each bacterial strain at each concentration were added to cell culture wells. Subsequently, the
141 culture medium was harvested and centrifuged at 200 rcf for 5 min to isolate THP-1 without
142 causing cell death. Supernatant was then centrifuged at 3000 rcf for 5 min to remove bacteria.
143 The resulting supernatant was analyzed for TNF-alpha response. TNF-alpha was measured using
144 an R&D Systems Quantikine ELISA Kit in a plate reader.
145
146 ***Animal models***
147 All animal experiments were approved by the Institutional Animal Care and Use Committee
148 (Columbia University, protocols ACAAAN8002 and AC-AAAZ4470). For tumor-bearing animals,
149 euthanasia was required when the tumor burden reaches 2 cm in diameter or after
150 recommendation by the veterinary staff. Mice were blindly randomized into various groups. Animal
151 experiments were performed on 8–12 weeks-old female BALB/c mice (Taconic Biosciences).
152 Tumor models were established with bilateral subcutaneous hind flank injection of mouse
153 colorectal carcinoma CT26 cells (ATCC) or mammary fat pad injection of 4T1-luciferase

154 mammary carcinoma cells (Kang, Princeton University). The concentration for implantation of the
155 tumor cells was 5×10^7 cells per ml in RPMI (no phenol red). Cells were injected at a volume of
156 100 µl per flank, with each implant consisting of 5×10^6 cells. Female transgenic MMTV-PyMT
157 mice (Jackson Laboratory) which develops mammary tumors were also used. Tumors were grown
158 to an average of approximately 200–400 mm^3 before experiments. Tumor volume was quantified
159 using calipers to measure the length, width, and height of each tumor ($V = L \times W \times H$). Because
160 z dimension of PyMT tumor is highly variable, total volume was calculated as length $\times$ width^2 $\times$
161 0.5. Volumes were normalized to pre-injection values to calculate relative or % tumor growth on
162 a per mouse basis.
163
164 ***Bacterial administration for in vivo experiments***
165 Overnight cultures of EcN, EcN *ΔkfiC*, and EcN iCAP were grown in LB medium with the
166 appropriate antibiotics and inducers. A 1:100 dilution in LB with appropriate antibiotics and
167 inducers was made the following day and grown in 37°C shaker until OD600 = 0.1–0.4 (mid-log
168 phase). Cultures were centrifuged at 3000 rcf for 10 min and washed three times with cold sterile
169 PBS. The bacteria were then normalized to a desired OD600. Unless otherwise noted,
170 intravenous injections were given through the tail-vein at the dose of 5×10^6 cells/mL (OD600 of
171 0.5) in PBS with a total volume of 100 µL per mouse. Intratumoral injections of bacteria were
172 performed at a concentration of 5×10^6 cells/mL with a total volume of 40 µL per tumor.
173 Intraperitoneal injections were injected at varying concentrations in PBS with a total volume of
174 100 µL per mouse. For induction of theta toxin production, AHL subcutaneous injection was given
175 to mice daily at 10 µM concentration with a total volume of 500 µL per mouse. For *in situ* activation
176 of iCAP, water containing 10 mM IPTG was given to mice a day after bacterial administration.
177
178 ***Biodistribution and in vivo animal imaging***
179 All bacterial strains used in this study had integrated *luxCDABE cassette* that could be visualized
180 by IVIS spectrum imaging system (Perkin Elmer) and were quantified by Living Image software.
181 Images and body weight of mouse were obtained every day starting the day of bacterial
182 administration until the study endpoint. At the study endpoint, mice were euthanatized by carbon
183 dioxide, and the tumors and organs (spleen, liver, and lungs) were extracted and imaged. They
184 were later weighed and homogenized using a gentleMACS tissue dissociator (C Tubes, Miltenyi
185 Biotec). Homogenates were serially diluted with sterile PBS and plated on LB agar plates with
186 erythromycin and incubated overnight at 37°C. Colonies were counted the next day.
187
188 ***Statistical analysis***
189 Statistical tests were performed either in GraphPad Prism 7.0 (Student's t-test and ANOVA) or
190 Microsoft Excel. The details of the statistical tests are indicated in the respective figure legends.
191 When data were approximately normally distributed, values were compared using either a
192 Student's t-test, one-way ANOVA for single variable, or a two-way ANOVA for two variables. Mice
193 were randomized into different groups before experiments.
194
195

References

1. Na, D.; Yoo, S. M.; Chung, H.; Park, H.; Park, J. H.; Lee, S. Y. Metabolic Engineering of Escherichia Coli Using Synthetic Small Regulatory RNAs. *Nature Biotechnology* **2013**, *31*, 170–174.

2. Yoo, S. M.; Na, D.; Lee, S. Y. Design and Use of Synthetic Regulatory Small RNAs to Control Gene Expression in Escherichia Coli. *Nature Protocols* **2013**, *8*, 1694–1707.

3. Datsenko, K. A.; Wanner, B. L. One-Step Inactivation of Chromosomal Genes in Escherichia Coli K-12 Using PCR Products. *Proceedings of the National Academy of Sciences* **2000**, *97*, 6640–6645.

4. Hsieh, P. F.; Lin, T. L.; Yang, F. L.; Wu, M. C.; Pan, Y. J.; Wu, S. H.; Wang, J. T. Lipopolysaccharide O1 Antigen Contributes to the Virulence in Klebsiella Pneumoniae Causing Pyogenic Liver Abscess. *PLoS ONE* **2012**, *7*.

5. Hsieh, P. F.; Lin, H. H.; Lin, T. L.; Chen, Y. Y.; Wang, J. T. Two T7-like Bacteriophages, K5-2 and K5-4, Each Encodes Two Capsule Depolymerases: Isolation and Functional Characterization. *Scientific Reports* **2017**, *7*.

6. Moller, H. J.; Heinegard, D.; Poulsen, J. H. Combined Alcian Blue and Silver Staining of Subnanogram Quantities of Proteoglycans and Glycosaminoglycans in Sodium Dodecyl Sulfate-Polyacrylamide Gels. *Analytical Biochemistry* **1993**, *209*, 169–175.

7. Zamze, S.; Martinez-Pomares, L.; Jones, H.; Taylor, P. R.; Stillion, R. J.; Gordon, S.; Wong, S. Y. C. Recognition of Bacterial Capsular Polysaccharides and Lipopolysaccharides by the Macrophage Mannose Receptor. *Journal of Biological Chemistry* **2002**, *277*, 41613–41623.

8. Hammerschmidt, S.; Wolff, S.; Hocke, A.; Rosseau, S.; Müller, E.; Rohde, M. Illustration of Pneumococcal Polysaccharide Capsule during Adherence and Invasion of Epithelial Cells. *Infection and Immunity* **2005**, *73*, 4653–4667.

9. Sokolovska, A.; Becker, C. E.; Stuart, L. M. Measurement of Phagocytosis, Phagosome Acidification, and Intracellular Killing of *Staphylococcus Aureus*. *Current Protocols in Immunology* **2012**, *99*, 14.30.1-14.30.12.

10. Drevets, D. A.; Canono, B. P.; Campbell, P. A. Measurement of Bacterial Ingestion and Killing by Macrophages. *Current Protocols in Immunology* **2015**, *109*, 14.6.1-14.6.17.